Modelling of single bubble-dynamics and thermal effects

D Papoulias[1], **M Gavaises**[2]

[1] CD-adapco, 200 Shepherds Bush Road, London W6 7NL, UK
[2] Department of Mechanical Engineering & Aeronautics, City University London, Northampton Square, London EC1V 0HB, UK

dimitrios.papoulias@cd-adapco.com

Abstract. This paper evaluates the solution effects of different Rayleigh-Plesset models (R-P) for simulating the growth/collapse dynamics and thermal behaviour of homogeneous gas bubbles. The flow inputs used for the discrete cavitation bubble calculations are obtained from Reynolds-averaged Navier-Stokes simulations (RANS), performed in high-pressure nozzle holes. Parametric 1-D results are presented for the classical thermal R-P equation [1] as well as for refined models which incorporated compressibility corrections and thermal effects [2, 3]. The thermal bubble model is coupled with the energy equation, which provides the temperature of the bubble as a function of conduction/convection and radiation heat-transfer mechanisms. For approximating gas pressure variations a high-order virial equation of state (EOS) was used, based on Helmholtz free energy principle [4]. The coded thermal R-P model was validated against experimental measurements [5] and model predictions [6] reported in single-bubble sonoluminescence (SBSL).

1. Introduction

Based on potential flow theory, Rayleigh and Plesset [7, 8] derived and tested the so-called Rayleigh-Plesset model for predicting the growth/collapse dynamics of cavitation bubbles. Since its inception, the R-P model has been further developed in order to compensate for the inherited assumptions of the method, which prohibit the physical realization of the violent bubble collapse phase. Inhomogeneous pressure effects developing upon the collapse of bubbles were addressed by Moss et al. [2]. To treat this model limitation, Moss introduced a time-derivative term of the gas-pressure in the classical R-P model, which effectively reproduced the rapid damping of the bubble collapse rebounds, as observed in SBSL experiments. Compressibility correction terms were formulated in the work of Keller and Miksis [3], and Lohse and Hilgenfeldt [5], as a function of the bubble's Mach number. The solution effects of the aforementioned compressible R-P models were examined by Prosperetti and Hao [9], assuming homogeneous bubbles and perfect-gas behavior. The Keller-Miksis R-P model was further extended in the work of Yasui [6], in order to also account for evaporation/condensation mass-transfer effects and chemical kinetics. For the calculation of the internal bubble gas-pressure, most of the aforementioned studies relied on idealized equations of state (EOS) or improved equations designed for real-gases, such as the second-order van der Waals model. Model limitations associated with the development of high gas-pressures, precursors of shock-waves in bubble sonoluminescence, were raised in the paper of Löfstedt et al. [10].

The thermal-bubble model proposed in this paper combines in an explicit way a multiparameter Helmholtz-type EOS, the energy equation and the R-P models presented in the reviewed studies. Details regarding the formulation of the implemented models are available in the following section.

2. Thermal bubble-dynamic R-P model

In the following analysis the Keller-Kiksis R-P equation (K-M) is presented, alongside to the suggested supplementary energy model for coupling the dynamic and thermal behavior of bubbles.

$$\left(1-\frac{\dot{R}}{c_L}\right)R\ddot{R}+\frac{3}{2}\left(1-\frac{\dot{R}}{3c_L}\right)\dot{R}^2=\frac{1}{\rho_L}\left(1+\frac{\dot{R}}{c_L}+\frac{R}{c_L}\frac{\mathrm{d}}{\mathrm{dt}}\right)\left[p_B-p_\infty-p_s(t)\right] \tag{1}$$

where R is the radius of the spherical bubble and the overdot symbol denotes time-derivative terms, i.e. bubble-wall velocity and acceleration. The bubble pressure p_B, the ambient static-pressure p_∞ and the imposed acoustic pressure-field p_s are collected inside the square brackets. Closure of equation (1) requires an additional expression for the dynamic boundary condition at the bubble-wall:

$$p_B = p_g - \frac{2\sigma}{R} - \frac{4\nu_L}{R}\dot{R} \tag{2}$$

equation (2) provides a relationship between the internal bubble gas-pressure p_g and the pressure acting on the external side of the bubble-wall. The remaining variables participating in equations (1) and (2) refer to the properties of the surrounding liquid-fluid, i.e. density ρ_L, speed of sound c_L, viscosity ν_L, and surface tension σ. These parameters are extrapolated from available correlations [11], for fixed pressure and temperature conditions.

The gas temperature of cavitating bubbles T_B is approximated by solving the energy equation:

$$\Delta U = m_B C_v \Delta T_B = -p_g \Delta V_B - kA_B \nabla T_B - hA_B\left(T_B - T_\infty\right) - \varepsilon\sigma A_B\left(T_B^4 - T_\infty^4\right) \tag{3}$$

equation (3) encapsulates variations of the internal energy ΔU of bubbles due to the growth/collapse pressure-volume work and the modeled heat-transfer mechanisms, i.e. convection, conduction and radiation. The variables m_B, V_B and A_B stand for the mass, volume and surface area of the bubble. The thermal conductivity k and heat-transfer coefficient h of the internal gas are calculated as functions of the Nusselt number [12]. In the thermal radiation term, σ corresponds to the Stefan-Boltzman constant and ε is the emissivity of the bubble, which is modeled as a black-body.

The gas pressure and temperature variables are coupled by integrating a Helmholtz virial EOS:

$$Z = \frac{\mathrm{p_g}}{\rho_g R_g T_B} = 1 + \delta\frac{\partial}{\partial\delta}\mathrm{a^r}(\delta,\tau) \tag{4}$$

the left-hand side in equation (4) is the ideal gas law, where R_g is the gas constant and ρ_g is the density. The right-hand side includes the residual Helmholtz energy α^r contribution to the ideal part, also known as compressibility coefficient Z, which is expressed as a multiparameter function of the reduced density δ and temperature τ. Similar virial expansion models are also used for estimating the heat-capacity C_v in equation (3).

Numerical integration of the formulated system of equations is performed iteratively, using the embedded fifth-order Runge-Kutta-Fehlberg algorithm and an adaptive step-size control with a minimum step of 1.0e-15 s. The bubble gas pressure and density unknowns in equation (4) are calculated by integrating successive Newton-Raphson iterations. The solution performance of the described thermal R-P models is examined in the forthcoming discussion, for sonoluminescence and cavitation bubble-dynamics.

3. Sonoluminescence and cavitation bubble-dynamics

Validation results of the implemented thermal R-P model are plotted in figure 1. The scatter dots in these graphs correspond to a) light-scattering measurements of the bubble-radius [5] and b) calculations of the gas temperature [6], while the solid lines are the equivalent predictions of the coded K-M bubble model. The reproduced SBSL case assumed a gas nucleus with initial size R_0 = 4.5 μm, which is perturbed from its equilibrium (T_∞ = 20 C and $p_{B,0} = p_\infty$ = 1 bar) by a pressure-wave (dashed line). The amplitude and frequency of the acoustic-wave are 1.35 bar and 20 kHz, respectively. As shown in these results, the gas bubble grows asymptotically during the rarefaction phase of the wave, driven by the low ambient pressure. Gradually, the pressure-field recovers to positive values causing the bubble to collapse. The bubble collapse-rate is decelerated by the internal gas, which is

compressed to high pressures and temperatures. Eventually, inertial effects force the bubble into repeatable growth/collapse rebound oscillations. Model predictions seem to be aligned with this sequence of dynamic events, both in terms of the measured bubble-radius and the corresponding prediction for the gas temperature. Löfstedt [5] calculated the peak temperature of this SBSL event to be ≈ 8500 K. Differences in the comparison of these results are noticed at the bubble's rebounds, mainly due to neglected physical mechanisms, e.g. mass-transfer and shock-waves effects [10].

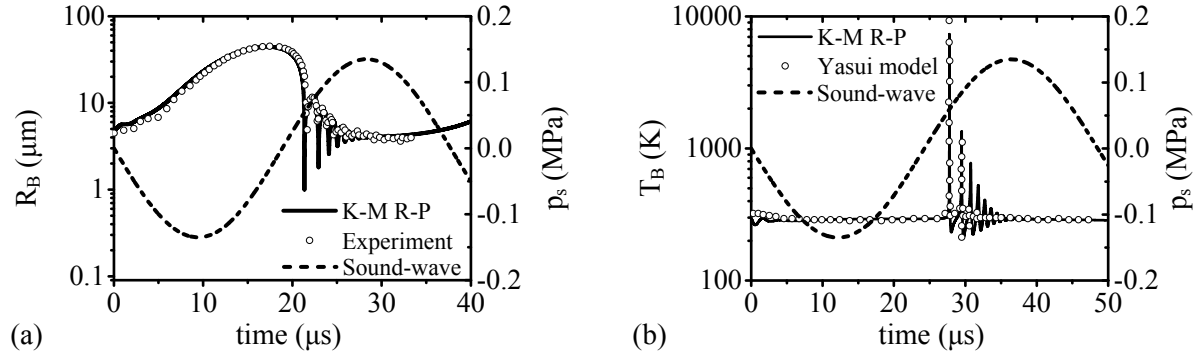

Figure 1. Validation of the thermal K-M model against reported a) experiments and b) predictions.

Additional single-bubble calculations are performed using the K-M and the classical thermal R-P equations as well as the compressible adiabatic model proposed by Moss. In these tests, the prescribed pressure boundary at the bubble-wall is extracted from incompressible single-phase RANS flow simulations inside a micro-sized nozzle (D = 200 μm). The pressure-drop applied to the water-liquid (T_∞ = 353 K) across the hole varied from 200 MPa at the inlet to 5 MPa at the outlet. The simulated cavitation nucleus is considered to be in equilibrium with the upstream flow, i.e. $p_{B,0}$ = 200 MPa and $T_{B,0}$ = 353 K, at an initial size equal to R_0 = 1 μm. Model predictions of the growth/collapse bubble-radius are plotted in figure 2 (a), as a function of the normalized spatial location x/L inside the hole where L is the length of the channel. In figure 2 (b) velocity and pressure contours of the internal flow are shown.

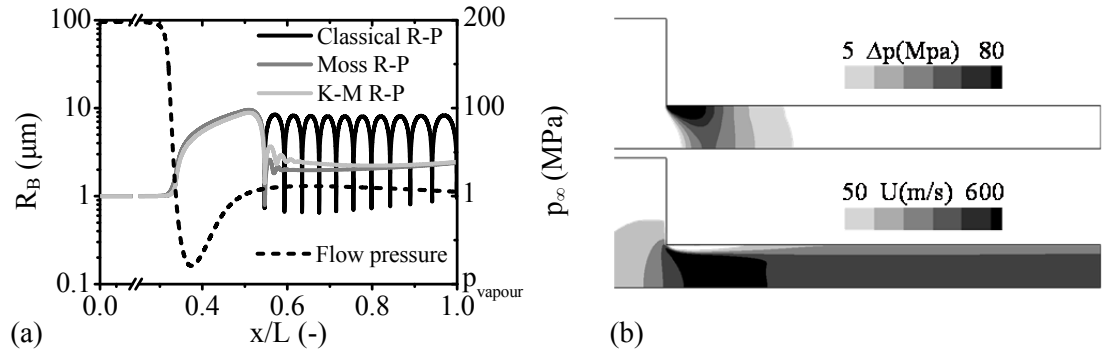

Figure 2. a) Cavitation growth/collapse dynamics calculated inside b) a high-pressure sharp nozzle.

Starting its journey from the upstream inlet, the gas nucleus arrives at the sharp hole step (x/L≈0.4) where it begins to grow due to the formed flow tension-site. The inception of the cavitation bubble is followed by a slow-rate asymptotic growth, which as it appears is equivalently predicted by the tested R-P models. This similarity implies that compressibility and thermal effects are insignificant during the initial growth phase. Further downstream (x/L≈ 0.55), the pressure is recovered (5 MPa) and the bubble is forced to implode. The bubble-dynamics ensuing after the termination of the growth phase are interpreted differently, depending on the utilized R-P equation. The compressible Moss and K-M models indicated a rapid decay of the cavitation oscillations, shortly after the collapse episode. On the contrary, the incompressible thermal R-P equation predicted repeatable rebounds with equally large amplitudes and consistent frequency. Damping in this case arises only from the viscous diffusion term.

Differences are also noticed in the predicted minimum bubble-radius, attained upon the initial collapse event. The thermodynamic behaviour of the cavitating bubble is depicted in figure 3.

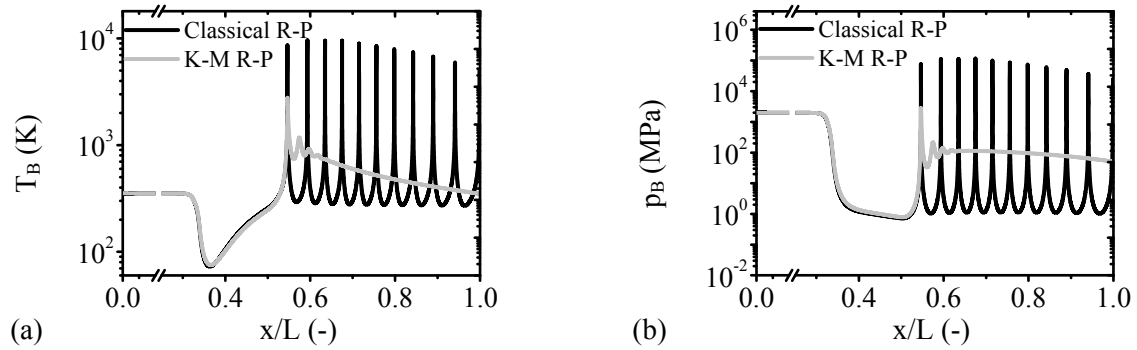

Figure 3. Homogeneous gas a) temperature and b) pressure predictions of the cavitation bubble.

Temperature and pressure variations of the cavitating gas-bubble are plotted for the thermal R-P models, i.e. the classical and K-M R-P equations. As seen in these graphs, during the initial asymptotic bubble-growth the internal gas is expanded to subatmospheric pressures and low temperatures. These conditions are promoted due to the absence of a mass-transfer model, i.e. evaporation effects. The development of hot-spots and high gas-pressures coincided with the locations where the bubble collapsed. The duration of these instances lasted only a few picoseconds, while their frequency of occurrence is a function of the damping terms integrated in each model. In absolute numbers, the classical thermal R-P model predicted temperatures and pressures in the order of 10000 K and 100 GPa, respectively. These values are considerably lower when the thermal K-M equation is used, ranging close to 3500 K and 0.5GPa.

4. Conclusions

In this paper a high-order Helmholtz EOS was coupled with different thermal R-P models. The method was validated against SBSL experiments and equivalent model predictions. Single-bubble cavitation dynamics were also calculated in high-pressure nozzle channels. The presented results indicated that during the violent implosion of bubbles the internal gas is elevated to high temperatures followed by pressures of the order of GPa. To proceed with the integration of bubble-dynamics within these physical limits, high-fidelity models are required for the characterization of the thermodynamic state variables and gas properties, as well as for addressing the role of shock-waves [13].

References

[1] Brennen C E 1995 *Cavitation and Bubble Dynamics* (New York: Oxford University Press)
[2] Moss W S, Levatin J L and Szeri A J 2000 *Proc. R. Soc. Lond.* A **456** 2983-94
[3] Keller J B and Miksis M 1980 *J. Acoust. Soc. Am.* **68**(2) 628-33
[4] Lemmon E W, Jacobsen R T, Penoncello S G and Friend D G 2000 *J. Phys. Chem. Ref. Data* **29** (3) 331-85
[5] Lohse D and Hilgenfeldt S 1997 *J. Chem. Phys.* **107**(17) 1359-62
[6] Yasui K 1997 *Phys. Rev.* E **56** (6) 6750-60
[7] Lord Rayleigh 1917 *Phil. Mag.* **34** 94-8
[8] Plesset M S 1949 *J. Appl. Mech.* **16** 277-82
[9] Prosperetti A and Hao Y 1999 *Phil. Trans. R. Soc. Lond.* A **357** 203-23
[10] Löfstedt R, Barber B P and Putterman S J 1993 *Phys. Fluids* A **5**(11) 2911-28
[11] Perry R H 1999 *Perry's Chemical Enginners' Handbook* (New York: McGraw-Hill)
[12] Incropera F P, Dewitt D P, Bergman T L and Lavine A S 2013 *Principles of Heat and Mass Transfer* (Singapore: John Wiley & Sons)
[13] Löfstedt R, Barber B P, R Hiller and Putterman S J 1992 *J. Acoust. Soc. Am.* **91**(1) 2331